

Discrete Synaptic Events Induce Global Oscillations in Balanced Neural Networks

Denis S. Goldobin^{1,2}, Matteo di Volo³, and Alessandro Torcini^{4,5,6,*}

¹*Institute of Continuous Media Mechanics, Ural Branch of RAS, Academician Korolev street 1, 614013 Perm, Russia*


²*Institute of Physics and Mathematics, Perm State University, Bukirev street 15, 614990 Perm, Russia*

³*Université Claude Bernard Lyon 1, Institut National de la Santé et de la Recherche Médicale, Stem Cell and Brain Research Institute U1208 Bron, France*

⁴*Laboratoire de Physique Théorique et Modélisation, CY Cergy Paris Université, CNRS, UMR 8089, 95302 Cergy-Pontoise cedex, France*

⁵*CNR—Consiglio Nazionale delle Ricerche—Istituto dei Sistemi Complessi, via Madonna del Piano 10, 50019 Sesto Fiorentino, Italy*

⁶*INFN Sezione di Firenze, Via Sansone 1, 50019 Sesto Fiorentino, Italy*

 (Received 10 November 2023; revised 5 June 2024; accepted 31 October 2024; published 6 December 2024)

Despite the fact that neural dynamics is triggered by discrete synaptic events, the neural response is usually obtained within the diffusion approximation representing the synaptic inputs as Gaussian noise. We derive a mean-field formalism encompassing synaptic shot noise for sparse balanced neural networks. For low (high) excitatory drive (inhibitory feedback) global oscillations emerge via continuous or hysteretic transitions, correctly predicted by our approach, but not from the diffusion approximation. At sufficiently low in-degrees the nature of these global oscillations changes from drift driven to cluster activation.

DOI: [10.1103/PhysRevLett.133.238401](https://doi.org/10.1103/PhysRevLett.133.238401)

Introduction—In several contexts the discrete nature of stochastic events should be taken into account to correctly predict the system dynamics. A typical example is represented by shot noise, which is conveyed by pulses and is therefore discontinuous, at variance with white noise, which is associated to thermal fluctuations and is continuous [1]. The inclusion of shot noise is fundamental to fully characterize the emergent phenomena in many fields of physics ranging from mesoscopic conductors [2] to driven granular gases [3].

The discrete nature of the events is an innate characteristic also of the neural dynamics, where a neuron receives inputs from other neurons via electrical pulses, that manifest as postsynaptic potentials (PSPs). The PSPs stimulating a neuron in the cortex are usually assumed to be uncorrelated with small amplitudes and high arrival rates. Therefore, the mean-field (MF) neural dynamics has been examined within the framework of the diffusion approximation (DA) [4,5] by treating synaptic inputs as a continuous Gaussian process.

However, several experiments have shown that rare PSPs of large amplitude can have a fundamental impact on the cortical activity [6,7] and that synaptic weight distributions display a long tail toward large amplitudes [8–10]. Furthermore, networks of inhibitory neurons with low connectivity (in-degree $K \simeq 30$ –80) have been identified in the cat visual cortex [11] and in the rat hippocampus [12],

where they are believed to be at the origin of global oscillations (GOs) in the γ band [13]. Moreover, the cortical connectivity is definitely more sparse in primates than in rodents as recently shown [14].

These experimental evidences call for the development of a MF formalism able to incorporate the effect of discrete synaptic events for diluted random neural networks. Population based formalisms, taking into account synaptic shot noise, have been previously developed for integrate-and-fire models [15–18]. However, such approaches are limited to stationary solutions and cannot describe the emergence of oscillatory behaviors.

In this Letter, we introduce a *complete* mean-field (CMF) approach for balanced neural networks [19,20], taking into account the sparseness of the network and the discreteness of the synaptic pulses, able to reproduce all the possible dynamical states. For simplicity, but without any loss of generality, we consider inhibitory balanced networks subject to an external excitatory drive [21–24].

Firstly, we illustrate that the DA fails in reproducing oscillatory dynamics in spiking neural networks for sufficiently low excitatory drive (high inhibitory feedback) by considering conductance- and current-based models. However, this regime is correctly reproduced by an MF approach whenever the sparse and discrete synaptic inputs are taken into account. Further, for quadratic integrate-and-fire (QIF) [25,26] networks via the CMF approach we obtain a complete bifurcation diagram encompassing asynchronous regimes (ARs) and oscillatory regimes (ORs), where individual neurons spike irregularly. The CMF

*Contact author: alessandro.torcini@cyu.fr

reveals subcritical and supercritical Hopf bifurcations from the AR to the OR as well as a region of coexistence of these two phases not captured by the DA [27]. Event-driven simulations of large QIF networks confirm the scenario predicted within the CMF theory. Furthermore, we show that the GOs, induced by discrete synaptic events can emerge due to two different mechanisms: cluster activation at sufficiently small K and drift driven at larger K .

Balanced network—As a prototype of a dynamically balanced system we consider a sparse inhibitory network made of N pulse-coupled neurons whose membrane potentials evolve according to the equations

$$\dot{v}_i(t) = F(v_i) + I - g \sum_{j=1}^N \sum_n \epsilon_{ji} \delta(t - t_j^{(n)}), \quad (1)$$

where I represents an external dc current, g the synaptic coupling, and the last term the inhibitory synaptic current. The latter is the linear superposition of instantaneous inhibitory PSPs emitted at times $t_j^{(n)}$ from the presynaptic neurons connected to neuron i . ϵ_{ji} is the adjacency matrix of the random network with entries 1 (0) if the connection from node j to i exists (or not), and we assume the same in-degree $K = \sum_j \epsilon_{ji}$ for all neurons. We consider two paradigmatic models of spiking neuron: the QIF with $F(v) = v^2$ [23–25,28,29], which is a current-based model of class I excitability, and the Morris-Lecar (ML) [30], a conductance-based model representing a class II excitable membrane [31]. The dc current and the synaptic coupling are assumed to scale as $I = i_0 \sqrt{K}$ and $g = g_0 / \sqrt{K}$ as usually done in order to ensure a self-sustained balanced state for sufficiently large K [19,22–24,39,40].

Mean-field description—For a sufficiently sparse network with $K \ll N$, the spike trains emitted by K presynaptic neurons can be assumed to be uncorrelated and Poissonian [20,21]; therefore the MF dynamics of a generic neuron can be represented in terms of the following Langevin equation:

$$\dot{V}(t) = F(V) + I - gS(t), \quad (2)$$

where $S(t)$ is a Poissonian train of δ spikes with rate $R(t) = K\nu(t)$, and $\nu(t)$ the population firing rate self-consistently estimated. Usually the Poissonian spike trains are approximated within the DA [4,5] as $S(t) = R(t) + \sqrt{R(t)}\xi(t)$, where $\xi(t)$ is a Gaussian white noise term. However, the DA can fail in reproducing the neural dynamics. Indeed, as shown in Fig. 1(a) for a sparse ML network, by employing the DA in (2) one obtains an asynchronous dynamics (blue curve), while the network evolution, characterized by GOs with frequency $f_c \simeq 18$ Hz (black dots), can be recovered only by explicitly taking into account the Poissonian spike trains in (2) (red line).

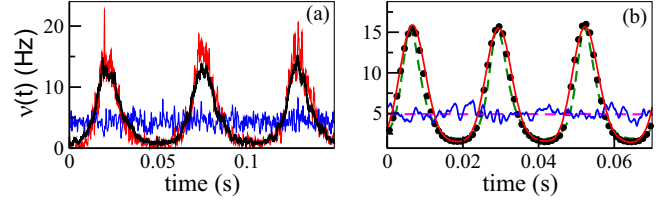


FIG. 1. Population firing rate $\nu(t)$ versus time for ML (a) and QIF (b) models. Black circles refer to network simulations, blue (red) solid line to diffusive (shot-noise) Langevin results obtained by integrating Eq. (2). In (b) magenta (green) dashed line denotes the DA (shot-noise) MF approximation resulting from the integration of Eq. (3) [Eq. (4)] for the QIF model; more details in [31]. The parameters for the ML model are $K = 20$, $i_0 = 0.1$, $g_0 = 5$, and network size $N = 20000$. Other parameters are reported in the Supplemental Material [31]. For the QIF model $K = 200$, $i_0 = 0.16$, $g_0 = 4$, and $N = 80000$ [41].

In the MF framework the population dynamics is usually described in terms of the membrane potential probability distribution function $P(V, t)$, whose time evolution for the QIF model is given [according to (2)] by the continuity equation,

$$\partial_t P(V, t) + \partial_V [(V^2 + I)P(V, t)] = R(t)\Delta P(V, T), \quad (3)$$

with boundary condition $\lim_{V \rightarrow \infty} V^2 P(V, t) = \nu(t)$ and where $\Delta P(V, T) = [P(V^+, t) - P(V, t)]$ with $V^+ = V + g$. By assuming that g is sufficiently small we can expand the latter term as $\Delta P(V, t) = \sum_{p=1}^{\infty} (g^p / p!) \partial_V^p P(V, t)$, and by limiting to the first two terms in this expansion we recover the DA corresponding to the following Fokker-Planck equation (FPE) [42]:

$$\partial_t P(V, t) + \partial_V \{ [V^2 + A(t)]P(V, t) \} = D(t) \partial_V^2 P(V, t), \quad (4)$$

where $A(t) = \sqrt{K}[i_0 - g_0\nu(t)]$ and $D(t) = g_0^2\nu(t)/2$. The DA can give incorrect predictions for the QIF model, as well. Indeed, as shown in Fig. 1(b) the network dynamics is oscillatory with $f_c \simeq 40$ Hz (black circles). This evolution is correctly captured by the MF equation (3) (green dashed line) and by the Langevin equation (2) driven by shot noise (red solid line). On the contrary, the FPE (4) (dashed magenta line) and the diffusive Langevin formulation (blue solid line) converge to a stable fixed point corresponding to asynchronous dynamics. Therefore, to reproduce the collective dynamical regimes observable in the network it is necessary to consider the continuity equation (3). In this respect we have developed a CMF formalism encompassing synaptic shot noise to identify the various possible regimes displayed by (3) and to analyze their stability.

The QIF model evolution can be transformed into that of a phase oscillator, the so-called θ neuron [25,32], by introducing the phase variable $\theta = 2 \arctan V$. However, this transformation has the drawback that even uncoupled

neurons are associated to a nonflat distribution of the phases, thus rendering it quite difficult to distinguish asynchronous from partially synchronized regimes [43,44]. A more appropriate phase transformation to analyze the synchronization phenomena is the following, $\psi = 2 \arctan(V/\sqrt{I}) \in [-\pi, \pi]$, which leads to a uniformly rotating phase in the absence of incoming pulses for suprathreshold neurons with $I > 0$ [31].

By considering the probability distribution of the phases $w(\psi, t) = P(V, t)(I + V^2)/(2\sqrt{I})$, Eq. (3) can be rewritten in terms of the so-called Kuramoto-Daido order parameters z_n [33,34] by expanding in Fourier space the distribution as $w(\psi, t) = (2\pi)^{-1} \sum_{n=-\infty}^{+\infty} z_n e^{-in\psi}$, with $z_0 = 1$ and $z_{-n} = z_n^*$. After laborious but straightforward calculations, one obtains the following evolution equations,

$$\dot{z}_n = i2n\sqrt{I}z_n + K\nu \left[\sum_{m=0}^{+\infty} I_{nm}(\alpha)z_m - z_n \right], \quad (5)$$

where $n = 1, 2, 3, \dots$, $\alpha \equiv g/\sqrt{I} = g_0/(\sqrt{i_0}K^{3/4})$, and the explicit expressions for $I_{nm}(\alpha)$ are reported in [31].

The firing rate can be self-consistently determined by the flux at the firing threshold $\lim_{V \rightarrow \infty} V^2 P(V, t) = 2\sqrt{I}w(\pi, t)$, as follows:

$$\nu = 2\sqrt{I}w(\pi, t) = \frac{\sqrt{I}}{\pi} \operatorname{Re} \left(1 + 2 \sum_{k=1}^{\infty} (-1)^k z_k \right). \quad (6)$$

The dynamics of the system (5) and (6) is controlled by only two parameters: K and α . Thus, we can limit to derive a bidimensional phase diagram in the plane $(i_0/g_0^2, K)$, that will comprehensively cover the entire diversity of the macroscopic regimes observable in the network. In particular, we have estimated the stationary solutions of Eqs. (5) and (6) by truncating the Fourier expansion in (5) to $M \geq 100$ modes in order to guarantee a numerical accuracy of $\mathcal{O}(10^{-12})$ for all the parameter values. The linear stability of the asynchronous state joined to the derivation of the corresponding amplitude equations (via a weakly nonlinear approach) has allowed us to identify the Hopf bifurcation (HB) line where the oscillatory dynamics emerges together with the supercritical or subcritical nature of the bifurcations (for more details, see Sec. S3 in [31]). The HB line obtained via the CMF (within the DA) is reported as an orange (black) line in Fig. 2(a). While the HBs are always supercritical within the DA, the HBs induced by the shot noise can be either supercritical (solid orange line) or subcritical (dashed orange line), thus allowing for regions where AR and OR coexist; see Fig. 2(b). A peculiarity of the CMF results is that the HB line is reentrant; thus, in a certain range of i_0/g_0^2 we have an AR only within a finite interval of in-degrees and GOs at sufficiently small and large K [as shown in

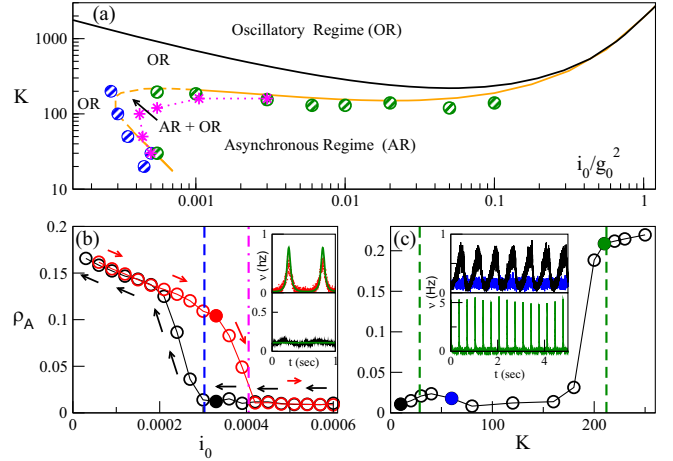


FIG. 2. (a) Phase diagram for the QIF network in the plane $(i_0/g_0^2, K)$. The black solid line is the supercritical HB line obtained within the DA, the orange solid (dashed) line is the supercritical (subcritical) HB line given by the CMF, the symbols refer to numerical estimations of the HBs and SNBs. The green (blue) circles denote HBs obtained by performing quasiadiabatic simulations by varying K (i_0) for constant i_0 (K) values, the magenta stars indicate SNBs. For more details, see Ref. [31]. (b), (c) Average order parameter ρ_A versus i_0 (K) for quasiadiabatic simulations. Black circles refer to decreasing (increasing) i_0 (K), while red circles refer to increasing i_0 . The blue dashed line in (b) denotes the subcritical HB given by the CMF, and the magenta dot-dashed line denotes the numerically estimated SNB. The two green dashed lines in (c) indicate the HBs given by the CMF. In the insets in (b) and (c) the population firing rates $\nu(t)$ versus time are reported for the states indicated by the corresponding colored filled circles. In the insets in (b) the results for the CMF (5) are also shown as green solid lines. The values of ρ_A in (b) [(c)] refer to $K = 100$ ($i_0 = 0.00055$) averaged over five network realizations, with $N = 80000$, for 30 s following a transient of 20 s. For all data, $g_0 = 1$ [41].

Fig. 2(c)]. As explained in the following, these two oscillatory regimes are due to different mechanisms.

Furthermore, there is a dramatic difference among the 2 MF approaches at small i_0 (large g_0): within the DA GOs are observable only above a critical K diverging to infinity for $i_0/g_0^2 \rightarrow 0$, while for the CMF analysis GOs are present at any K value for $i_0/g_0^2 < 0.00029$.

Network simulations—In order to verify the CMF predictions we have performed essentially exact numerical simulations of QIF networks, according to (1), by employing an event-driven integration scheme [35], which allowed us to follow the network dynamics for long times, up to 50–100 sec, for system of sizes $N = 10000 - 80000$ [31]. In particular, to characterize the macroscopic evolution of the network we measured the indicator introduced in [45] $\rho = (\sigma_V^2/\sigma_i^2)^{1/2}$, where $\sigma_i^2 = \langle v_i^2 \rangle - \langle v_i \rangle^2$ and σ_V is the standard deviation of the mean membrane potential $\bar{V} = \sum_{i=1}^N v_i/N$, with $\tau(\langle \cdot \rangle)$ denoting an ensemble (a time) average. A coherent (asynchronous) macroscopic activity is

characterized by a value of ρ remaining finite (vanishing as $\rho \propto N^{-1/2}$) for $N \rightarrow \infty$ [24,46]. The actual value of ρ is related to the level of synchronization among the neurons: perfect synchrony to $\rho \equiv 1$.

A finite size analysis of the order parameter ρ_A averaged over several different network realizations has allowed us to identify the HBs and the saddle-node bifurcations (SNBs) of limit cycles displayed in Fig. 2 [31]. In particular, in Fig. 2(a) green (blue) circles refer to HBs identified via quasiadiabatic simulations by varying K (i_0) for constant i_0 (K) values, while the magenta stars indicate SNBs. Numerical simulations are in good agreement with the CMF results and allowed us also the identification of a coexistence region for asynchronous and oscillatory collective dynamics. A hysteretic transition from AR to OR obtained by varying quasiadiabatically i_0 is displayed in Fig. 2(b); the coexistence region can be clearly identified between the subcritical HB (blue dashed line) and the SNB (magenta dashed line). Two coexisting solutions are reported in the insets of Fig. 2(b) confirming the good agreement between CMF (green lines) and the network simulations (red and black lines). Furthermore, as shown in Fig. 2(c) for sufficiently small i_0/g_0^2 values GOs are observable at small ($K \leq 30$) and large ($K \geq 200$) in-degrees, while the AR is present only at intermediate in-degrees ($K \in [40:180]$). The dynamics in these three intervals is visualized by reporting in the insets of Fig. 2(c) the firing rates $\nu(t)$ at $K = 10$ (black line), $K = 60$ (blue line), and $K = 210$ (green line).

In large part of the phase diagram (namely, for $i_0/g_0^2 < 0.2$), both in the AR and OR we observe an irregular firing activity of the neurons associated to mean coefficient of variations $\overline{CV} \simeq \mathcal{O}(1)$ [36], as expected in sparse balanced networks.

Two kinds of GO—As previously mentioned, we can identify two classes of GOs induced by discrete synaptic events in the interval $i_0/g_0^2 \in [0.00036:0.00070]$. Their difference is already clear by considering the MF membrane potential evolution $V_0(t)$ given by the following *zeroth-order* Langevin equation for the QIF:

$$\dot{V}_0(t) = V_0^2 + \sqrt{K}[i_0 - g_0\nu(t)] = V_0^2 + A(t), \quad (7)$$

where current fluctuations have been neglected and $\nu(t)$ is the population firing induced by the shot noise. Whenever $A < 0$ ($A > 0$) the QIF model displays excitable dynamics (periodic firing) [26]. The GOs reported in the insets of Fig. 2(c) for $K = 10$ [$K = 210$] are characterized by $A(t)$ always negative [positive for large part of the oscillation period] as shown in Fig. 3(a) [Fig. 3(b)] (lower panels). Therefore, for $K = 10$ [$K = 210$] $V_0(t)$ displays subthreshold oscillations [large excursions from negative to positive values driven by $A(t) > 0$] as shown in the upper panel of Fig. 3(a) [Fig. 3(b)].

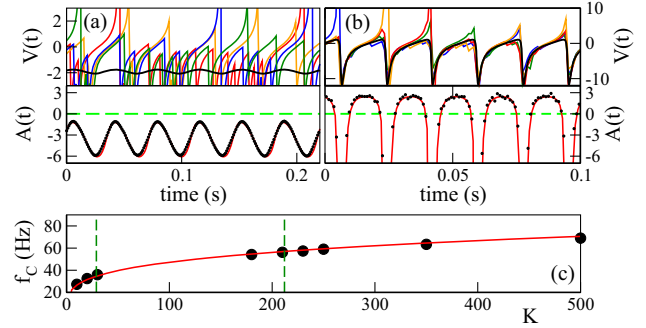


FIG. 3. (a),(b) Lower panels: effective input current $A(t)$ versus time. Red lines (black dots) refer to CMF (network simulations) results. Upper panels: membrane potential evolution in time. Black lines (other colors) refer to $V_0(t)$ (single neuron dynamics). (c) Frequency of the GOs f_c (black circles) versus K . The red solid line refers to f_0 . Green vertical dashed lines have the same meaning as in Fig. 2(c). Data correspond to $i_0/g_0^2 = 0.00055$ (with $g_0 = 20$), to $K = 10$ (a) and $K = 210$ (b), network simulations to $N = 80000$ [41].

As shown in Fig. 2(c), the low (high) in-degree GOs are characterized by a low (high) level of coherence among the neurons; this is confirmed by the evolution of the membrane potentials $v_i(t)$ of four generic neurons reported in Figs. 3(a) and 3(b). In both cases the neurons spike irregularly [47]; however, for $K = 210$ the single neurons $v_i(t)$ essentially follow the MF evolution $V_0(t)$, while for $K = 10$ their dynamics is quite uncorrelated.

These behaviors can be explained by two different mechanisms once it is noticed that for both cases the GO frequency f_c is extremely close to the firing frequency of an isolated neuron $f_0 = 1/T_0 = \sqrt{I}/\pi$; see Fig. 3(c). This suggests that at a first approximation the GOs are due to the neurons not receiving any inhibitory PSP from reset to threshold. For low K , whenever a neuron fires large amplitude inhibitory PSPs are delivered. These induce a transient synchronization in the K postsynaptic neurons and a subgroup, not receiving further PSPs, can eventually reach threshold together at a time $\simeq T_0$. This transient synchronizing effect of small clusters of neurons (termed *cluster activation* [48]) is at the basis of the GOs observable for $K = 10$ in Fig. 2(c). For increasing K , the amplitude of the PSPs decreases; therefore, above some critical in-degree ($K \simeq 30$ in this case) a single inhibitory PSP is no longer able to induce a sufficiently strong synchronizing effect on the postsynaptic neurons and the dynamics becomes asynchronous [as shown in Fig. 2(c)].

For larger K , the postsynaptic neurons receive several small inhibitory PSPs at each population burst; whenever K is sufficiently large a non-negligible part of the neurons can get synchronized by the discharge of inhibitory PSPs. As shown in Fig. 3(b), the time courses of the membrane potentials are now extremely coherent by approaching the threshold, where fluctuations lead to irregular firing of the neurons. However, a sufficient percentage of neurons *drift*

driven is always able to fire together with a period $\simeq T_0$ giving rise to the GOs.

Conclusions—We have shown that the macroscopic phase diagram of balanced networks is strongly influenced by the discreteness and the finite amplitude of PSPs. In particular, we have developed a CMF formalism by including Poissonian shot noise which reproduces quite well the network simulations, at variance with the DA. This scenario is robust and extends beyond instantaneous synapses to exponentially decaying PSPs, as shown in Fig. S4 in [31].

Our analysis of balanced inhibitory networks has revealed the existence of two kinds of GOs induced by discrete synaptic events, thus completing the previous scenario based on the DA [21,27]. Furthermore, we have shown that GOs can emerge even in extremely sparse inhibitory networks with frequencies going from 1–2 Hz (δ band) to 100 Hz (γ band), thus providing theoretical support for the supposition reported in [13] that the γ oscillations observed in the hippocampus are generated by subnetworks of interneurons with low in-degrees $K \simeq 30$ –80 [12].

The CMF approach is valid in sparse networks for $K \ll N$. Whenever $K \simeq \mathcal{O}(N)$ the correlations among the spike trains reaching the neuron should be taken into account, an extension of the CMF in this direction will be worth future investigations. The effect of finite N fluctuations has been analyzed in globally coupled QIF networks [51,52]; it will be interesting to extend such approach to random networks. Finally, the CMF formalism can be generalized to neural systems with delay and synaptic kinetics as shown in Sec. S3.G in [31]; this will be the subject of future studies.

Acknowledgments—We acknowledge stimulating discussions with Alberto Bacci, Alberto Ferrara, Nina La Miciotta, Lyudmila Klimentko, Gianluigi Mongillo, Simona Olmi, and Antonio Politi. We are also grateful to the anonymous referees for extremely useful suggestions. D. S. G. acknowledges the support of the CNR Short Term Mobility Programme 2021 for a visit to Istituto dei Sistemi Complessi, Sesto Fiorentino, Italy, where part of this work was developed. A. T. received financial support by the Labex MME-DII (Grant No. ANR-11-LBX-0023-01), by CY Generations (Grant No. ANR-21-EXES-0008), and together with M. d. V. by the ANR Project ERMUNDY (Grant No. ANR-18-CE37-0014). M. d. V. also received support by the Labex CORTEX (Grant No. ANR-11-LABX-0042) of Université Claude Bernard Lyon 1 and by the ANR via the Junior Professor Chair in Computational Neurosciences Lyon 1.

-
- [1] W. Schottky, *Ann. Phys. (Berlin)* **362**, 541 (1918).
 [2] Y. M. Blanter and M. Büttiker, *Phys. Rep.* **336**, 1 (2000).
 [3] D. Lucente, M. Viale, A. Gnoli, A. Puglisi, and A. Vulpiani, *Phys. Rev. Lett.* **131**, 078201 (2023).

- [4] R. Capocelli and L. Ricciardi, *Kybernetik* **8**, 214 (1971).
 [5] H. C. Tuckwell, *Introduction to Theoretical Neurobiology: Nonlinear and Stochastic Theories* (Cambridge University Press, Cambridge, England, 1988), Vol. 2.
 [6] S. Song, P. J. Sjöström, M. Reigl, S. Nelson, and D. B. Chklovskii, *PLoS Biol.* **3**, e68 (2005).
 [7] S. Lefort, C. Tomm, J.-C. F. Sarria, and C. C. Petersen, *Neuron* **61**, 301 (2009).
 [8] R. Miles, *J. Physiol.* **431**, 659 (1990).
 [9] B. Barbour, N. Brunel, V. Hakim, and J.-P. Nadal, *Trends Neurosci.* **30**, 622 (2007).
 [10] G. Buzsáki and K. Mizuseki, *Nat. Rev. Neurosci.* **15**, 264 (2014).
 [11] Z. F. Kisvárdy, C. Beaulieu, and U. T. Eysel, *J. Comp. Neurol.* **327**, 398 (1993).
 [12] A. Sik, M. Penttonen, A. Ylinen, and G. Buzsáki, *J. Neurosci.* **15**, 6651 (1995).
 [13] G. Buzsáki and X.-J. Wang, *Annu. Rev. Neurosci.* **35**, 203 (2012).
 [14] G. A. Wildenberg, M. R. Rosen, J. Lundell, D. Paukner, D. J. Freedman, and N. Kasthuri, *Cell Rep.* **36** (2021).
 [15] M. J. E. Richardson and R. Swarbrick, *Phys. Rev. Lett.* **105**, 178102 (2010).
 [16] R. Iyer, V. Menon, M. Buice, C. Koch, and S. Mihalas, *PLoS Comput. Biol.* **9**, e1003248 (2013).
 [17] S. Olmi, D. Angulo-Garcia, A. Imparato, and A. Torcini, *Sci. Rep.* **7**, 1577 (2017).
 [18] F. Droste and B. Lindner, *J. Comput. Neurosci.* **43**, 81 (2017).
 [19] C. van Vreeswijk and H. Sompolinsky, *Science* **274**, 1724 (1996).
 [20] N. Brunel, *J. Comput. Neurosci.* **8**, 183 (2000).
 [21] N. Brunel and V. Hakim, *Neural Comput.* **11**, 1621 (1999).
 [22] J. Kadmon and H. Sompolinsky, *Phys. Rev. X* **5**, 041030 (2015).
 [23] M. Monteforte and F. Wolf, *Phys. Rev. Lett.* **105**, 268104 (2010).
 [24] M. di Volo and A. Torcini, *Phys. Rev. Lett.* **121**, 128301 (2018).
 [25] G. B. Ermentrout and N. Kopell, *SIAM J. Appl. Math.* **46**, 233 (1986).
 [26] B. Gutkin, *Encyclopedia of Computational Neuroscience* (Springer, New York, 2022), pp. 3412–3419.
 [27] M. Di Volo, M. Segneri, D. S. Goldobin, A. Politi, and A. Torcini, *Chaos* **32**, 023120 (2022).
 [28] C. R. Laing, *J. Math. Neurosci.* **8**, 4 (2018).
 [29] I. Ratas and K. Pyragas, *Phys. Rev. E* **100**, 052211 (2019).
 [30] C. Morris and H. Lecar, *Biophys. J.* **35**, 193 (1981).
 [31] See Supplemental Material at <http://link.aps.org/supplemental/10.1103/PhysRevLett.133.238401>, which includes Refs. [24,25,32–38], for details on the employed models, the integration of the neural networks as well as of the population models, and on the CMF approach.
 [32] B. Ermentrout, *Scholarpedia* **3**, 1398 (2008), revision no. 122134.
 [33] Y. Kuramoto, *Chemical Oscillations, Waves, and Turbulence* (Springer Science & Business Media, Berlin, Heidelberg, New York, Tokyo, 2012), Vol. 19.
 [34] H. Daido, *Prog. Theor. Phys.* **88**, 1213 (1992).

- [35] A. Tonnelier, H. Belmabrouk, and D. Martinez, *Neural Comput.* **19**, 3226 (2007).
- [36] The coefficient of variation $cv(i)$ for the neuron i is the ratio between the standard deviation and the mean of the interspike intervals associated with its firing activity. \overline{CV} is the ensemble average of the single neurons $cv(i)$.
- [37] A. Torcini and P. Politi, *Eur. Phys. J. B* **25**, 519 (2002).
- [38] R. Albert and A.-L. Barabási, *Rev. Mod. Phys.* **74**, 47 (2002).
- [39] A. Renart, J. de la Rocha, P. Bartho, L. Hollender, N. Parga, A. Reyes, and K.D. Harris, *Science* **327**, 587 (2010).
- [40] A. Litwin-Kumar and B. Doiron, *Nat. Neurosci.* **15**, 1498 (2012).
- [41] The times (frequencies) are reported in physical units by assuming a membrane time constant $\tau_m = 10$ ms.
- [42] E. Haskell, D. Q. Nykamp, and D. Tranchina, *Network* **12**, 141 (2001).
- [43] B. Kralemann, L. Cimponeriu, M. Rosenblum, A. Pikovsky, and R. Mrowka, *Phys. Rev. E* **76**, 055201(R) (2007).
- [44] A. V. Dolmatova, D. S. Goldobin, and A. Pikovsky, *Phys. Rev. E* **96**, 062204 (2017).
- [45] D. Golomb, *Scholarpedia* **2**, 1347 (2007).
- [46] E. Ullner and A. Politi, *Phys. Rev. X* **6**, 011015 (2016).
- [47] The value of \overline{CV} is $\simeq 0.8-0.9$ in the whole range of in-degrees $K \in [10:500]$ for $i_0/g_0^2 = 0.00055$ [36].
- [48] Cluster activation is not related to clustering instabilities observable in noisy globally coupled neural networks [49,50].
- [49] N. Brunel and D. Hansel, *Neural Comput.* **18**, 1066 (2006).
- [50] Y. Feld, A. K. Hartmann, and A. Torcini, *New J. Phys.* **26**, 063017 (2024).
- [51] V. V. Klinshov and S. Y. Kirillov, *Phys. Rev. E* **106**, L062302 (2022).
- [52] V. Klinshov, P. Smelov, and S. Y. Kirillov, *Chaos* **33**, 061101 (2023).